Resonant Plasma Heating by Electrostatic and Alfven Waves

Liu Chen[1], Zhihong Lin[2], Roscoe White[2]

[1]*Department of Physics and Astronomy, University of California, Irvine CA. 92697*

[2]*Plasma Physics Laboratory, Princeton University, P.O.Box 451,*

Princeton, New Jersey 08543

Resonant heating of particles in waves of large amplitude is considered. It is shown that adiabatic invariants are easily broken with large amplitude waves, even at frequencies normally considered nonresonant. An electrostatic wave of large amplitude propagating perpendicular to a confining uniform magnetic field is shown to produce significant perpendicular stochastic heating with the wave frequency a fraction of the cyclotron frequency. Similarly, large amplitude Alfven waves with wave frequencies a small fraction of the cyclotron frequency are shown to produce significant particle heating, bringing particles to speeds comparable to the Alfven velocity in a few hundred cyclotron periods.

PACS numbers: 52.35.Fp 52.50.Gj

I. INTRODUCTION

Resonant heating of particles in a magnetic field is a subject which has been examined by many authors and is of importance in the heating of magnetically confined laboratory as well as extraterrestrial plasmas. For a review see Lichtenberg and Lieberman [2]. The transition from adiabatic to stochastic heating was first examined by Nekrasov [3], Jaeger and Lichtenberg [4], and Lieberman and Lichtenberg [5]. Stochastic heating by a lower hybrid wave in a tokamak was investigated by Karney [8] for wave frequency much larger than the cyclotron frequency. It has been previously noted [6,7] that heating with ion Bernstein waves (IBW) can be obtained at frequencies above the cyclotron frequency Ω but below the second harmonic, at frequencies of $\omega/\Omega = 3/2,\;\; 4/3$, etc., but to our knowledge a breaking of the invariance of the magnetic moment at frequencies well below the cyclotron frequency has never been reported in a theoretical work. Neither have we been able to find a clear experimental search for such heating in an experiment. In this Letter we wish to demonstrate that at sufficiently large wave amplitude this is indeed possible.

II. CYCLOTRON HEATING

Consider the simplest cyclotron heating problem possible, that of a particle gyrating in a constant magnetic field, acted upon by an electrostatic plane wave propagating perpendicular to the field.

The Hamiltonian for this system is

$$H = \frac{(\vec{v} - \vec{A})^2}{2} + \Phi(x,t) \tag{1}$$

with the magnetic field given by the vector potential $\vec{A} = -By\hat{x}$, giving equations of motion

$$\dot{v}_x = Bv_y - \partial_x \Phi, \qquad \dot{v}_y = -Bv_x - \partial_y \Phi \tag{2}$$

Take the units of time to be given by Ω, the cyclotron frequency, and let the electrostatic wave be given by a single harmonic, $\Phi = \Phi_0 cos(kx - \omega t)$. There are then three dimensionless parameters characterizing the heating problem. Define $\rho = v/\Omega$ to be the instantaneous cyclotron radius. Then $k\rho$ characterizes the ratio of cyclotron radius to wave length, $k^2\Phi_0$ characterizes the ratio of particle displacement in the wave to wave length, and ω/Ω the ratio of the wave frequency to the cyclotron frequency. The initial particle distribution is also characterized by $k\rho_0$ with ρ_0 a mean cyclotron radius for the distribution.

The equations of motion become $\dot{v}_x = v_y + k\Phi_0 sin(kx - \omega t), \quad v_y = -x + x_0$, giving

$$\frac{d^2x}{dt^2} + x = x_0 + k\Phi_0 sin(kx - \omega t) \tag{3}$$

For small wave amplitude at the cyclotron frequency it is possible to describe the particle response to the wave in terms of oscillation at the cyclotron frequency with a slowly varying cyclotron radius, or energy. In the case of interest here wave amplitudes are large and wave frequencies different from, but comparable to, the cyclotron frequency, so response of the particle at additional frequencies must be retained. To treat the full problem it is necessary to include particle motion at fractions of the cyclotron frequency, sidebands, harmonics, etc. The particle motion must be written $x = x_0 + \lambda cos(t) - \mu sin(t) + \sum_m [\alpha_m cos(\nu_m t) + \beta_m sin(\nu_m t)]$ with λ, μ, α_m, β_m slowly varying in time compared to $1, \nu_m$, with ν_m giving the set of frequencies necessary to describe the motion. A full analytic treatment is not possible, but some analytic approximations give some insight into the nature of the solutions.

First consider Eq. 18 for $ks \equiv k(x - x_0) \ll 1$. Letting $2T = kx_0 - \omega t$ and keeping only lowest order in ks we have

$$\frac{d^2s}{dT^2} + \left[\frac{4}{\omega^2} - \frac{4k^2\Phi_0}{\omega^2} cos(2T)\right] s = k\Phi_0 \omega sin(2T) \tag{4}$$

ie, a driven Mathieu equation with unstable solutions for $\omega \simeq 2/q$ with q integer. Of course this equation is valid only for small ks, but it indicates the existence of large amplitude solutions for these values of ω.

Now consider a Poincaré section of $k\rho$, $\psi = kx - \omega t$, by taking points when $v_y = 0, \dot{v}_y > 0$. This gives $\psi = \psi_0 - \omega t_j$, with $\psi_0 = kx_0$, and t_j given by the times at which $x = x_0$ and $\dot{x} < 0$. Given $\lambda(t)$, $\mu(t)$, $\alpha_m(t)$, $\beta_m(t)$ one can solve for the Poincaré times t_j. Without loss of generality at $t = 0$ we take x random, v_x random negative and $v_y = 0$, giving $x = x_0$, $\psi(0) = \psi_0$. The values at $t = 0$ then determine one Poincaré point. Others are given by $k\rho(t_j)$, $\psi(t_j) = \psi_0 - \omega t_j$. Fixed points are given by $dv/dt = 0$ and constant phase, or $\dot{\lambda} = \dot{\mu} = \dot{\alpha_m} = \dot{\beta_m} = 0$.

In general these equations are very complicated and the Poincaré section must be examined numerically. For significant heating there must exist resonances. A complete analysis would consist of a determination of all fixed points and then the calculation of the widths of the islands occuring around the elliptic points, followed by an estimate of stochastic threshold due to island overlap. Unfortunately this approach is not feasible, and to make any progress analytically one must be guided by numerical results. A numerical Poincaré plot using Eq. 18 is shown in Fig. 1 for $k^2\Phi_0 = 0.1$, $\omega = 1/2$, showing period two fixed points occuring at small wave amplitude. In Fig. 2 are shown these two fixed point orbits. The nature of the resonance is obvious, a particle at the fixed point completes two cyclotron periods while completing one wave period. The first fixed point orbit shows a large variation of the orbit between one cyclotron period and the second, in the second orbit this modification is clearly higher order. In examining the orbits recall that the initial point $x = x_0$ is a Poincare point, and since $v_y = x_0 - x$ all Poincare points occur at $x = x_0$, but only if $\dot{x} < 0$. Thus for both orbits the Poincare points are at the bottom of the two circles, with very different y values in one case and almost the same in the other.

Guided by numerical results, including a Fourier analysis of the fixed point trajectories, we illustrate the nature of the solutions for this case by considering only the cyclotron motion and the particle response at the wave frequency of $\omega = 1/2$. Employing multiple time scales, express the solution to the equations of motion as $x = x_0 + \lambda cos(t) - \mu sin(t) + \alpha cos(\omega t) - \beta sin(\omega t)$ with $\lambda, \mu, \alpha, \beta$ slowly varying with respect to $1, \omega$. We then find, keeping only leading order in the slow time scale and using $e^{\pm i a sin(b)} = \sum_m J_m(a) e^{\pm i m b}$,

$$\begin{aligned}-2\frac{d\mu}{dt}cos(t) - 2\frac{d\lambda}{dt}sin(t) + (1-\omega^2)\alpha cos(\omega t) - (1-\omega^2)\beta sin(\omega t) = \\ k\Phi_0 \sum_{jklm} J_j(k\lambda)J_k(k\mu)J_l(k\alpha)J_m(k\beta) sin[(j-k+l\omega-m\omega-\omega)t] cos[\psi_0 + (j+l)\pi/2] \\ +k\Phi_0 \sum_{jklm} J_j(k\lambda)J_k(k\mu)J_l(k\alpha)J_m(k\beta) cos[(j-k+l\omega-m\omega-\omega)t] sin[\psi_0 + (j+l)\pi/2]\end{aligned} \tag{5}$$

Taking the frequency to be a fraction of the cyclotron frequency, $\omega = 2/q$ with q an integer and integrating over the short time scales we have

$$(1-\omega^2)\alpha = k\Phi_0 \sum_{jklm} J_j(k\lambda)J_k(k\mu)J_l(k\alpha)J_m(k\beta) sin(\psi_0 + (j+l)\pi/2)\Delta_{\omega+} \tag{6}$$

$$(1-\omega^2)\beta = k\Phi_0 \sum_{jklm} J_j(k\lambda)J_k(k\mu)J_l(k\alpha)J_m(k\beta) cos(\psi_0 + (j+l)\pi/2)\Delta_{\omega-} \tag{7}$$

$$2\frac{d\mu}{dt} = -k\Phi_0 \sum_{jklm} J_j(k\lambda)J_k(k\mu)J_l(k\alpha)J_m(k\beta) sin(\psi_0 + (j+l)\pi/2)\Delta_{1+} \tag{8}$$

$$2\frac{d\lambda}{dt} = -k\Phi_0 \sum_{jklm} J_j(k\lambda)J_k(k\mu)J_l(k\alpha)J_m(k\beta) cos(\psi_0 + (j+l)\pi/2)\Delta_{1-} \tag{9}$$

with $\Delta_{\zeta\pm} = \delta_{j-k+(l-m-1)\omega,\zeta} \pm \delta_{j-k+(l-m-1)\omega,-\zeta}$.

To gain an intuitive understanding of the occurences of the nonlinear resonances which permit heating at frequencies well below the cyclotron frequency we can examine the limit of small wave amplitude, $k^2\Phi_0 \ll 1$ analytically. Then we have $k\alpha \ll 1$, $k\beta \ll 1$.

Now set $\omega = 1/2$. To the leading orders in $k\alpha$ and $k\beta$ we then find the first delta function of $\Delta_{\omega\pm}$ is limited to the values $(j,k,l,m) = (s, s-1, 0, 0)$ and the second delta function to $(s, s, 0, 0)$, with s integer. Similarly, for $\Delta_{1\pm}$, the first delta function is limited to the values $(j,k,l,m) = (s, s-1, 1, 0)$, $(s, s-1, 0, -1)$, $(s, s-$

$2,-1,0)$, $(s,s-2,0,1)$, with s integer, and the second delta function to the values $(j,k,l,m)=(s,s+1,1,0)$, $(s,s+1,0,-1)$, $(s,s,-1,0)$, $(s,s,0,1)$, with s integer. Note that these values are peculiar to the case of $\omega=1/2$, which is a special degenerate case since $\omega=1/2$ is the only solution to $1-\omega=\omega$. There are fewer but different lowest order terms for other fractions. Now in each term replacing the sum $s=-\infty,\infty$ with $s=2n,2n+1$, $n=-\infty,\infty$, denoting $C_0=cos(\psi_0)$, $S_0=sin(\psi_0)$, and defining $F_{a,b}(\lambda,\mu)=\sum_{n=-\infty}^{\infty}(-1)^n J_{2n+a}(k\lambda)J_{2n+b}(k\mu)$, we have

$$(1-\omega^2)\alpha=k\Phi_0[C_0(F_{1,0}+F_{1,1})+S_0(F_{0,0}+F_{0,-1})], \tag{10}$$

$$(1-\omega^2)\beta=k\Phi_0[C_0(F_{0,0}-F_{0,-1})+S_0(F_{1,0}-F_{1,1})], \tag{11}$$

$$\begin{aligned}-2\frac{d\mu}{dt}&=k\Phi_0 J_1(k\alpha)[C_0(F_{0,-1}+F_{0,-2}+F_{0,1}+F_{0,0})-S_0(F_{1,0}+F_{1,-1}+F_{1,2}+F_{1,1})]\\&+k\Phi_0 J_1(k\beta)[C_0(-F_{1,0}+F_{1,-1}-F_{1,2}+F_{1,1})+S_0(-F_{0,-1}+F_{0,-2}-F_{0,1}+F_{0,0})],\end{aligned} \tag{12}$$

$$\begin{aligned}2\frac{d\lambda}{dt}&=k\Phi_0 J_1(k\alpha)[S_0(F_{0,-1}+F_{0,-2}+F_{0,1}-F_{0,0})+C_0(F_{1,0}+F_{1,-1}+F_{1,2}+F_{1,1})]\\&+k\Phi_0 J_1(k\beta)[S_0(-F_{1,0}+F_{1,-1}+F_{1,2}-F_{1,1})+C_0(F_{0,-1}-F_{0,-2}-F_{0,1}+F_{0,0})].\end{aligned} \tag{13}$$

These equations determine the motion of a Poincaré point in the $k\rho$, ψ plane for small $k^2\Phi_0$. To determine the existence of resonances first look for fixed points of the Poincaré map, with $k^2\Phi_0\ll 1$. In this case α and β are small, and since $\lambda(0)=-\alpha(0)$ and for a fixed point λ must be constant, it remains small. Keeping only up to first order in λ we find for the existence of a fixed point in the case $\omega=1/2$ either $C_0=0$ or $S_0=0$.

For $C_0=1, S_0=0$ we have

$$(1-\omega^2)\alpha=k\Phi_0 J_1(k\lambda)[J_2(k\mu)+J_0(k\mu)], \tag{14}$$

$$(1-\omega^2)\beta=-k\Phi_0[J_1(k\mu)+J_0(k\mu)], \tag{15}$$

$$\begin{aligned}0&=J_1(k\lambda)[J_0(k\mu)+J_2(k\mu)][J_2(k\mu)+J_0(k\mu)]\\&-J_1(k\lambda)[J_1(k\mu)+J_0(k\mu)][2J_0(k\mu)+2J_2(k\mu)+J_1(k\mu)+J_3(k\mu)],\end{aligned} \tag{16}$$

$$\begin{aligned}0&=J_1^2(k\lambda)[J_0(k\mu)+J_2(k\mu)][2J_0(k\mu)+2J_2(k\mu)-J_1(k\mu)-J_3(k\mu)]\\&+[J_1(k\mu)+J_0(k\mu)][-2J_1(k\mu)-J_2(k\mu)+J_0(k\mu)].\end{aligned} \tag{17}$$

To lowest order in λ, μ is given by $0 = [J_1(k\mu) + J_0(k\mu)][-2J_1(k\mu) - J_2(k\mu) + J_0(k\mu)]$. The first root is from $J_0 = 2J_1 + J_2$ giving $k\mu = 0.825$. Equation 16 then gives $\lambda = 0$, and we find $\alpha = 0$, $\beta = -1.62k\Phi_0$. Since $\lambda = \alpha = 0$, the Poincaré points are given by $t_j = 2j\pi$. The fixed points are then $k\rho = k(\mu - \omega\beta)$, $\psi = 0$ and $k\rho = k(\mu + \omega\beta)$, $\psi = \pi$, as seen in Fig. 1.

No solution is found for $C_0 = 0, S_0 = 1$. The second pair of fixed points in Fig. 1 at $\psi = \pm\pi/2$ and $k\rho = 1.84$ is more complex, due to a combination of motion at ω and 3ω. It should be obvious from the above that by including particle response at more frequencies, and allowing larger values of $k^2\Phi_0$ the number of fixed points in the map will increase enormously.

For $\omega \neq 1/2$ but less than 1, the situation is qualitatively different. To leading order there do not exist any fixed points; rather the fixed points of the map emerge from $\rho = 0$ as the coalescence of complex conjugate pairs as Φ_0 is increased. Nevertheless, such fixed points exist for all integer q, associated with the unstable domains of the associated Mathieu equation. A numerical Poincaré plot is shown in Fig. 3 for $k^2\Phi_0 = 0.1$, $\omega = 1/3$, showing period three fixed points which move upward as $k^2\Phi_0$ increases. In Fig. 4 is shown the fixed point orbit at for $\omega = 1/3$. Again the motion is easily interpreted as consisting of three cyclotron oscillations within one wave oscillation. The orbit initiates at the orgin, with $\dot{x} < 0$, which is one Poincare point. The three cyclotron periods consist of 1) the left half of the lower ellipse, continuing around to the bottom of the small central ellipse, which is another Poincare point, 2) the upper ellipse, returning again to the bottom of the small central ellipse, which is the second Poincare point, and 3) the right half of the lower ellipse, returning to the origin.

In Fig. 5 is shown the Poincare plot for $\omega = 1/4$, $k^2\Phi_0 = 0.6$. Although at first glance there appear to be four O-points in this plot, there are only two. The islands with centers near $\psi = \pm\pi/2$ in fact have no O-points, they still exist only as a complex conjugate pair. In Fig. 6 is shown the fixed point orbit for the same parameters. There are four cyclotron periods contained in the wave period, but $v_y = 0$ is reached only for two of them, the other two are at the waist of the violin, where x becomes small but does not reach $x = x_0$. The fixed points are the origin and the bottom of the small ellipse at the top of the orbit, where $\dot{x} < 0$.

In Fig. 7 is shown the Poincare plot for $\omega = 1/4$, and slightly larger wave amplitude, $k^2\Phi_0 = .77$. There are now four fixed points in the Poincare plot. Note also that the map has become very chaotic. In Fig. 8 is shown the fixed point orbit for the same parameters. The cyclotron periods are; 1) starting at the origin, traversing the left side of the upper violin and ending at the bottom of the two small upper ellipses, 2) continuing onto the smaller of the two small upper ellipses, and down the right side of the lower violin, to the lowest point on the orbit, 3) the left side of the lower violin, again ending at the bottom of the two small upper ellipses, and 4) around the larger of the two upper ellipses and down the right side of the upper violin to the origin. The two narrow violin waists are two additional conjugate pairs of fixed points waiting to be born.

In Fig. 9 is shown fixed points for $\omega = 1/5$, $k^2\Phi_0 = 0.5$. In this plot there is only one O-point, the other four exist as complex conjugate pairs awaiting birth. In Fig. 10 is shown the fixed point orbit for the same parameters, the only Poincare point being the origin.

In Fig. 11 is shown a Poincare plot for $\omega = 2/5$, $k^2\Phi_0 = .2$. There are four fixed points, but only one of them is real. Its pair can be seen as an island at $\psi = \pm\pi$. The other two consists of a pair of conjugate roots which cannot be seen. In Fig. 12 is shown the fixed point orbit for the same parameters, with the origin being the only Poincare point.

In Fig. 13 is shown a Poincare plot for $\omega = 2/5$, $k^2\Phi_0 = .6$. There are four fixed points, and now two of them are real. The other two islands can be seen at $\psi = \pm\pi/2$. In Fig. 14 is shown the fixed point orbit for the same parameters, with the origin and the bottom of the small upper ellipse being the Poincare points.

In Fig. 15 is shown the Poincare plot for $\omega = 1/10$, $k^2\Phi_0 = .6$. Only one O-point exists, at $\psi = 0$. In Fig. 16 is shown the fixed point orbit for the same parameters, and in Fig. 17 is shown the orbit x(t). Periodic motion in the wave takes 10 cyclotron periods, the smaller oscillations are due to the cyclotron motion, but $x = 0$ with $\dot{x} < 0$ only at the origin. If the wave amplitude is increased enough to make all the O-points real the map is completely stochastic.

In Fig. 18 is shown the stochastic domain for $\omega = 1/10$, $k^2\Phi_0 = 1.$. A wave of this amplitude stochasticizes the motion at any frequency, although the extent of the stochastic domain is smaller for smaller frequencies. At low frequencies smaller islands are compensated by the fact that there are more of them.

Now investigate the approach to chaos and the extent of the chaotic domain, which limits the possible heating obtained. In Figs. 19, 20 21 is shown the increase of the stochastic domain, bounded by good KAM surfaces at large $k\rho$, as $k^2\Phi_0$ is increased, for $\omega = 1/2$. The good KAM surfaces are in the domain in which the perpendicular energy is only oscillatory, described by the magnetic moment, which is an adiabatic invariant, as is well known to occur for large energy and weak field [4]. The extent of the stochastic domain increases in discrete jumps as new resonances overlap and domains around them become stochastic. Fig. 21 shows the occurance of such a step, as the stochastic domain steps around a new period three resonance. Heating of an initially cold distribution proceeds to the maximum limit given by the good KAM surfaces in a rather short time; on the order of one to two hundred cyclotron periods. Even at a wave frequency of 1/10 of the cyclotron frequency a Poincaré plot is quite stochastic for $k^2\Phi_0 = 1$. Note that this is a collisionless result.

In Figure 22 is shown the extent of the stochastic domain in $k\rho$ versus $k^2\Phi_0$ and the speed with which an initially cold distribution is heated for $\omega = 1/2$. This figure was obtained by initiating 100 orbits distributed in x with $k\rho < 0.1$ and advancing to T = a) $10/\Omega$, b) $100/\Omega$, and c) $1000/\Omega$. the final curve c) is the limit determined by the remaining KAM surfaces and a longer run does not change the extent of the domain.

In Figure ?? is shown the variation of the extent of the stochastic domain in $k\rho$ versus $k^2\Phi_0$ as a function of wave frequency. Curve a) is given by heating at the cyclotron frequency, b) at half the cyclotron frequency, and c) at 1/5 the cyclotron frequency. Note that for small wave amplitude heating at the cyclotron frequency is clearly more efficient, but that for large amplitude heating at a lower frequency can be almost as effective.

Finally Figure 24 shows the variation of the extent of the heating domain in $k\rho$ versus wave frequency for $k^2\Phi_0 =$ 0.36, 0.8, and 2.6. For smaller wave amplitude some peaking can indeed be seen at low-order (small) integer fractions, as predicted by the Mathieu equation approximation. As the amplitude increases, however, nonlinear generation of many fixed points smooths out the resonance structures and makes the extent of the domain almost linear in ω.

The change in the Fourier spectrum of the orbits is shown in Figs. 25 - 28 for $\omega = 1/2$. A rapid increase in the number of harmonics as Φ_0 is increased is observed.

III. ALFVEN WAVE HEATING

The Alfvèn wave is a fundamental excitation of a magnetically confined plasma. Alfvèn waves, either excited spontaneously or by external sources, have been observed or predicted to be present in plasmas ranging from laboratory to space and astrophysical environments. Interactions between Alfvèn waves and charged particles thus play crucial roles in many plasma dynamical processes. The present work deals with the issue of pitch angle scattering and energization of charged particles (ions) by finite amplitude Alfvèn waves. Previous theoretical investigations of heating mechanisms have nearly always been based on the existence of the primary cyclotron resonance, ie $\omega - k_z u_z \pm n\Omega_c \simeq 0$ where ω and $\vec{k}$ are respectively the angular frequency and wave vector of the Alfvèn wave, $\vec{B}_0 = B_0\hat{z}$ is the confining magnetic field, $\Omega_c = qB_0/mc$ is the cyclotron frequency, $\vec{u}$ is the laboratory frame particle velocity, $n \geq 1$ and

$\pm$ corresponds to right (+) and left (−) circular polarization*. Such resonances will change the magnetic moment $\mu = u_\perp^2/2B_0$ leading to pitch angle scattering and heating. Here $\vec{u}_\perp$ is the velocity perpendicular to $\vec{B}_0$. Since for the Alfvèn waves $\omega \simeq k_z v_A$ with $v_A = B/(4\pi n_0 m_i)^{1/2}$ the Alfvèn velocity, the cyclotron resonance condition becomes $k_z v_z = k_z(u_z - v_A) \simeq \pm n\Omega_c$, where $\vec{v}$ is the particle velocity in the wave frame. Noting that typically $|k_z v_A| < |n\Omega_c|$ the resonance condition generally requires that u_z be super Alfvènic at least. Recognizing that this condition is often not satisfied, Wu and coworkers [?] have examined nonlinear interactions between ions and Alfvèn waves under nonresonant conditions using a one dimensional ($\vec{k} = k_z\hat{z}$) model. Their results, in part motivating our present work, indicate that while the Alfvèn waves can lead to large amplitude oscillations in the ion motion, there is no stochastic heating. The fact that finite $\vec{k}_\perp$ is necessary for stochastic heating has also been observed in simulations [?], but for cases in which the cyclotron resonance condition was satisfied.

In this Letter we find that given a sufficiently large amplitude, obliquely propagating wave ($\vec{k} = k_z\hat{z} + \vec{k}_\perp$), there indeed exists efficient stochastic ion pitch angle scattering and heating by the Alfvèn wave even when $k_z u_z$ is only a small fraction of Ω_c. Note for cold ions this means $\omega \ll \Omega_c$.

The physics of this stochastic heating is similar to that due to a perpendicularly propagating electrostatic wave with a frequency a small fraction of Ω_c reported in a recent publication [1]. To demonstrate the similarity consider a linearly polarized Alfvèn wave in the laboratory frame X, Y, Z, given by $\vec{B}_w = B_w \hat{y} cos(\psi - \omega t)$ with $\psi = \vec{k} \cdot \vec{X}$ and $\omega = k_z v_A$. Take the units of time to be given by Ω_c, the cyclotron frequency, and normalize the field to B_0. In the wave frame x, y, z we have $\psi = k_x x + k_z z$ and the velocity v is constant in time. Dimensionless numbers characterizing the problem are then $k_x v$, $k_z v$, and the wave magnitude B_w/B_0.

The equations of motion become $\dot{v}_x = v_y - v_z B_w cos\psi$, $\quad v_y = x_0 - x$, $\quad \dot{v}_z = v_x B_w cos\psi$, giving

$$\frac{d^2 x}{dt^2} + x = x_0 - v_z B_w cos\psi. \tag{18}$$

and the instantaneous location of a particle in phase space is given by x, z and the pitch $\lambda = v_z/v$.

To first order in B_w we have $d^2x/dt^2 + x = x_0 - \lambda(0) v B_w cos\psi$ and $d\lambda/dt = v_x v B_w cos\psi$. This equation is equivalent to that studied previously for cyclotron heating [1], with $k_z v_z/\Omega_c = k_z v\lambda(0)/\Omega_c$ playing the role of the frequency of

*In the present case the $n = 0$ resonance relies on the compressional component of the wave magnetic field, which is generally small and negligible. Furthermore, this $n = 0$ resonance does not change μ and only energizes particles along $\vec{B}_0$ and hence is not of interest here.

the electrostatic wave ω, and $k_x v\lambda(0)B_w/(B_0\Omega_c)$ the nonlinearity parameter. Thus for small B_w we expect the same resonances as found in that analysis, although for larger values of B_w the approximation of $\lambda = \lambda(0)$ will be invalid in the differential equation for x and the motion will be more complex.

To study the resonances, take a Poincaré section of λ, ψ, formed by taking points when $v_y = 0$ and $\dot{v}_y > 0$. In Fig. 29 is shown a sample Poincaré plot with $k_x v = 0.1$, $B_w = 0.22$, and there are resonances at $k_z v_z = 2/n$ for all small n values, although not all are visible in this plot. The corresponding electrostatic wave frequency [1] is $\omega = k_z v_z$ so the period two fixed points at $k_z v_z = \pm.5$ correspond to $\omega = 1/2$, the period three resonances at $k_z v_z = \pm 1/3$ corresponds to $\omega = 1/3$, etc. The plot is symmetric between positive and negative pitch as expected for a plane polarized wave. At larger amplitude these resonances of course produce stochastic motion, and hence allow change in pitch λ. Transformed to the laboratory frame such a change in pitch is equivalent to particle heating, and it is this heating of cold particles by Alfvèn waves which we wish to investigate. In Fig. 30 is shown a Poincaré plot at slightly larger amplitude, with $k_x v = 0.1$, $k_z v = 1$, $B_w = 0.3$. A wave of this amplitude clearly allows stochastic motion from pitch $\lambda = -1$ to $\lambda = 1$ and thus in the rest frame can energize particles up to speeds of twice the Alfvèn velocity.

Also of interest for Alfvèn waves propagating in interstellar space, consider a left circularly polarized Alfvèn wave, again in the wave frame, given by $\vec{B}_w = -B_w\hat{x}cos(\alpha)sin(\psi) + B_w\hat{y}cos\psi + B_w\hat{z}sin(\alpha)sin(\psi)$ with $\psi = k_x x + k_z z$ and $tan(\alpha) = k_x/k_z$. In the laboratory frame this is a right moving wave, and cold particles, as seen in the wave frame, all have $v_z/v = -1$. In Fig. 31 is shown a Poincaré plot for a circularly polarized wave with $k_x v = 0.1$, $k_z v = 0.5$, $B_w = 0.3$. Although the surfaces are more distorted than in the case of a plane polarized wave, and no longer symmetric in the sign of v_z, one can clearly see some resonances. At this amplitude much of the plot is chaotic, and particles can freely move from $v_z/v = -1$ to $v_z/v \simeq 0.4$. Thus in the rest frame the particle distribution has a velocity which is a significant fraction of the Alfvèn speed.

In Fig. 32 is shown the maximum pitch λ_{max} of a distribution initiated at $\lambda = -1$, after 100 cyclotron periods, for a circularly polarized wave, for a) $k_x v = 0.1$, $k_z v = 0.5$, and b) $k_x v = 0.2$, $k_z v = 0.5$. The average λ is about half the maximum. Thus for $B_w \simeq 0.5$ the distribution is accelerated to a velocity on the order of the Alfvèn velocity.

In Fig. 33 is shown the maximum pitch λ_{max} of a distribution initiated at $\lambda = -1$, after 100 cyclotron periods, for a circularly polarized wave, for $k_x/k_z = 0.2$ with a) $B_w = 0.1$, b) $B_w = 0.3$, and c) $B_w = 0.6$.

IV. CONCLUSION

In conclusion, we have demonstrated that significant perpendicular heating can be obtained well below the cydlotron frequency. This process may have application in laboratory heating devices as well as in astrophysical situations. We have also shown that large amplitude Alfvèn waves can energize cold ions even when the wave frequency is well below the ion cyclotron frequency. This result may have significance for the heating of ions in the solar corona.

This work was supported by the U.S. Department of Energy Grant DE-FG03-94ER54271 and under contract number DE-AC02-76-CHO3073 and NSF Grant ATM-9971529. The authors acknowledge useful discussions with Fulvio Zonca.

---

[1] L. Chen, Z. Lin and R. B. White *Phys. Rev. Lett.* **xx**, xx (2001).

[2] M. A. Lieberman and A. J. Lichtenberg *Regular and Chaotic Dynamics* Springer Verlag, New York (1983).

[3] A. K. Nekrasov *Nucl. Fusion* **10**, 387 (1970).

[4] F. Jaeger and A. J. Lichtenberg *Ann. Phys.* **71**, 319 (1972).

[5] M. A. Lieberman and A. J. Lichtenberg *Plasma Physics* **15**, 125 (1973).

[6] H. Abe, H. Okada, R. Itatani, M. Ono, and H. Okuda *Phys. Rev. Lett.* **53**, 1153 (1984).

[7] H. Abe, H. Momota, R. Itatani, A. Fukuyama *Phys. Fluids.* **23**, 2417 (1980).

[8] C.F.F. Karney *Phys. Fluids.* **22**, 2188 (1979).

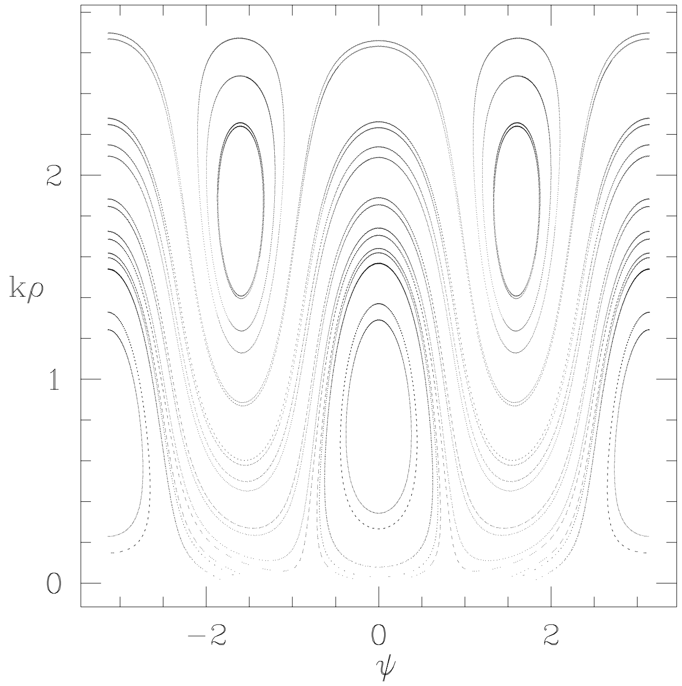

FIG. 1. Poincare, k=1, $\Phi_0 = .1$, $\omega = 1/2$

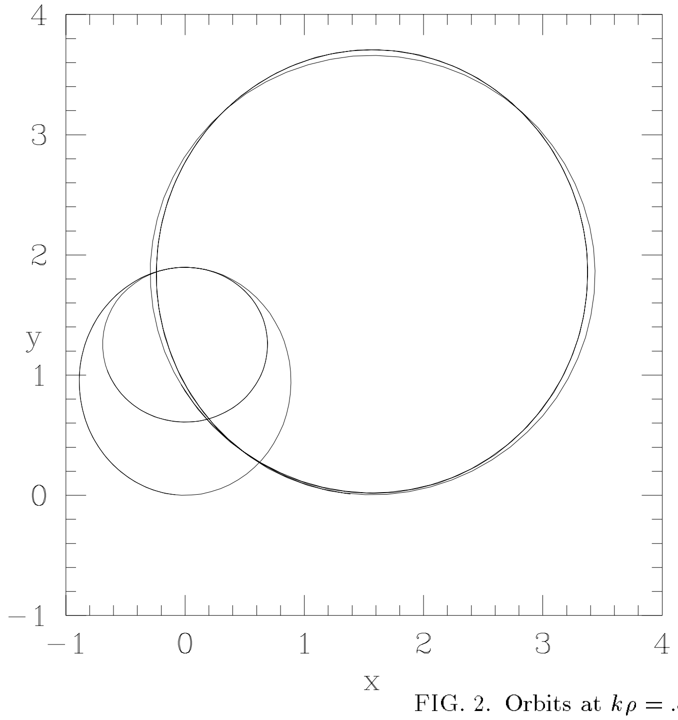

FIG. 2. Orbits at $k\rho = .825, 1.841$ fixed points

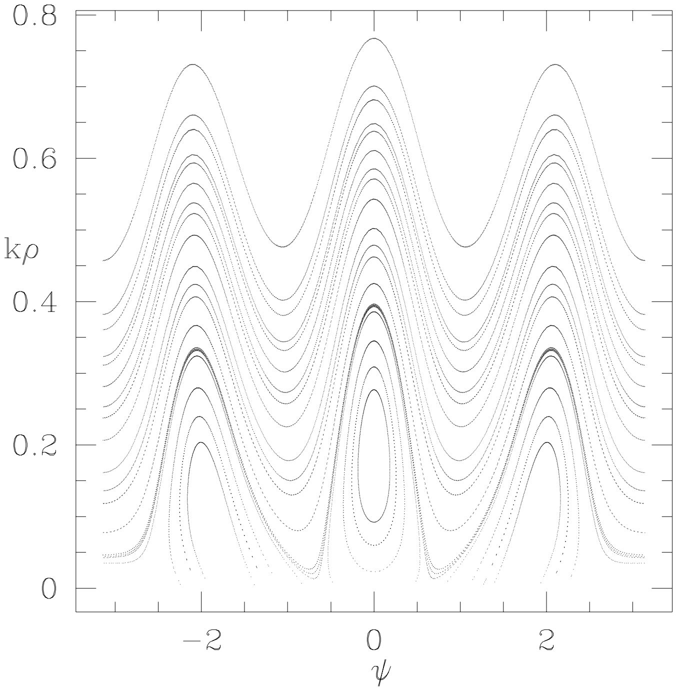

FIG. 3. Poincare, $k^2\Phi_0 = .1$, $\omega = 1/3$

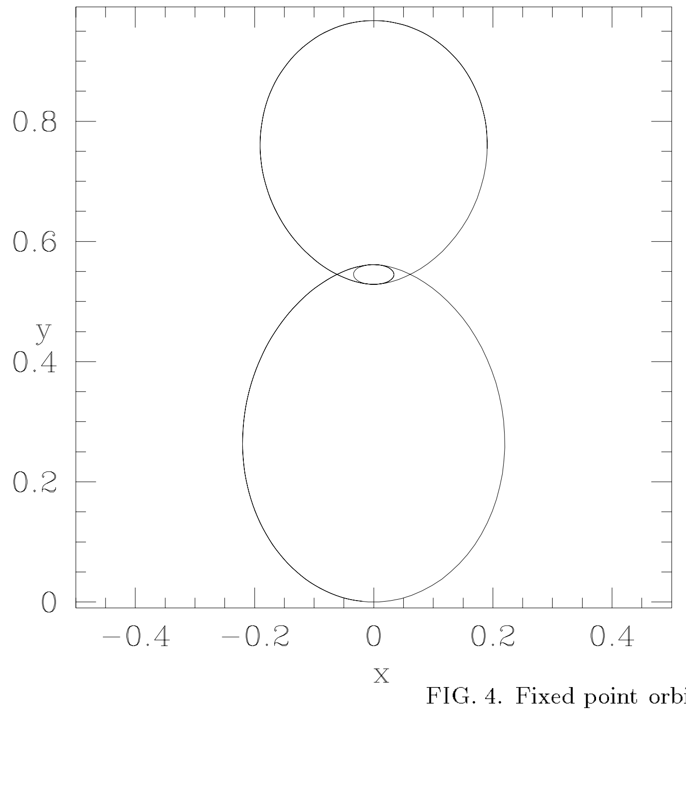

FIG. 4. Fixed point orbit, $k^2\Phi_0 = .1$, $\omega = 1/3$

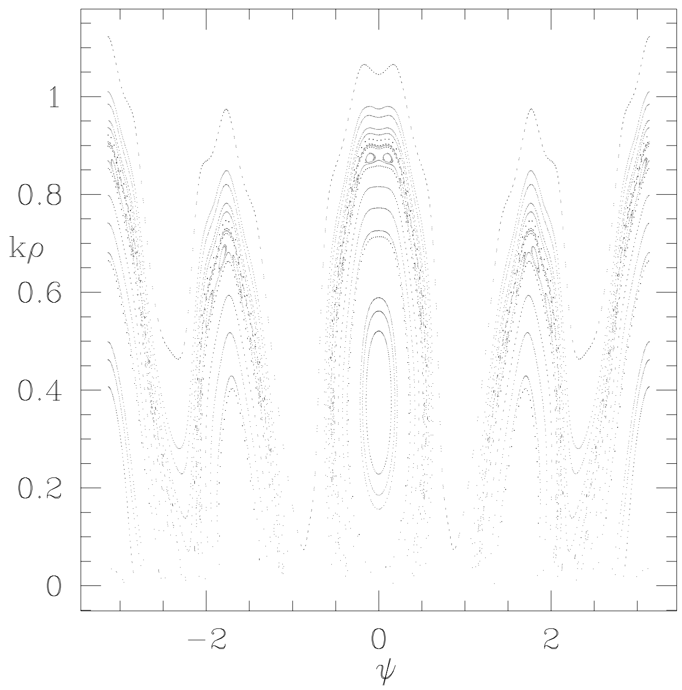

FIG. 5. Poincare, $k^2\Phi_0 = .6$, $\omega = 1/4$

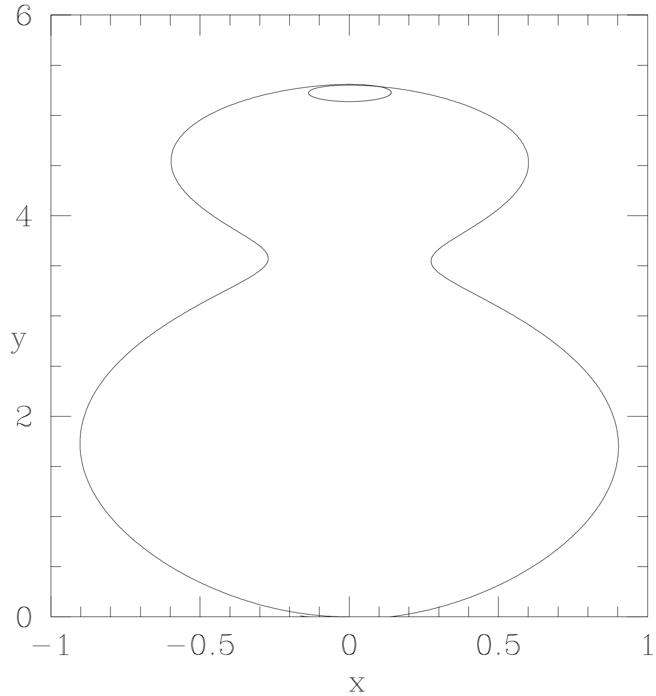

FIG. 6. Fixed point orbit, $k^2\Phi_0 = .6$, $\omega = 1/4$

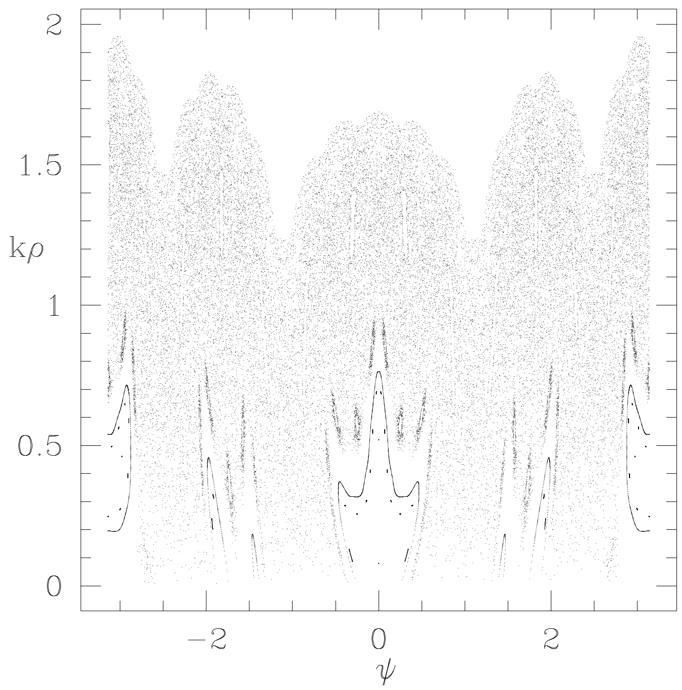

FIG. 7. Poincare, $k^2\Phi_0 = .77$, $\omega = 1/4$

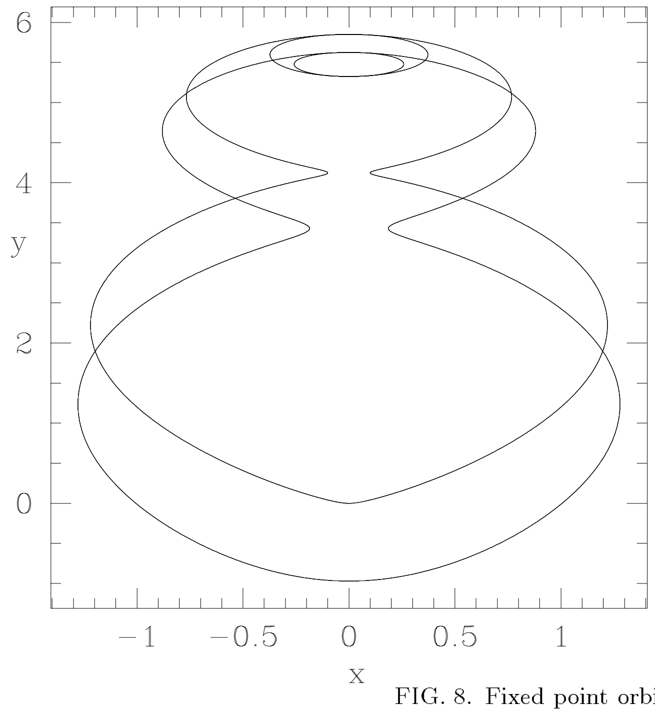

FIG. 8. Fixed point orbit, $k^2\Phi_0 = .77$, $\omega = 1/4$

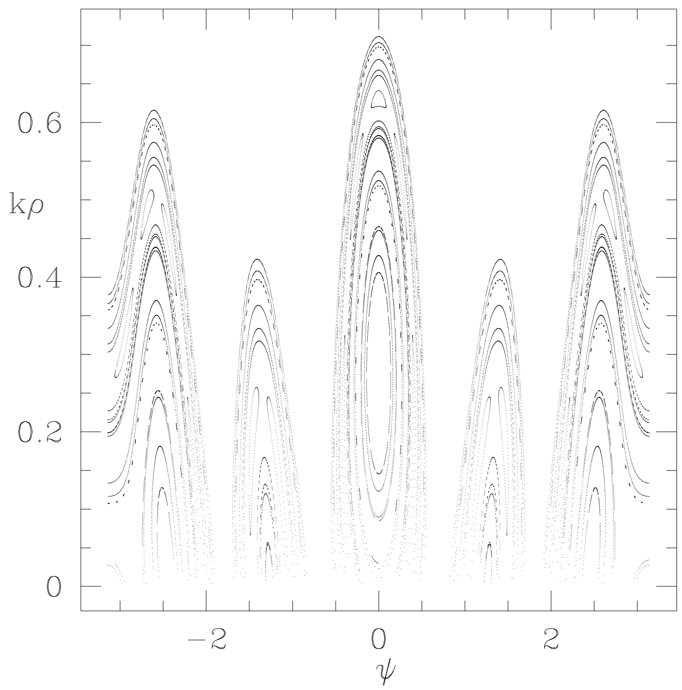

FIG. 9. Poincare, $k^2\Phi_0 = 0.5$, $\omega = 1/5$

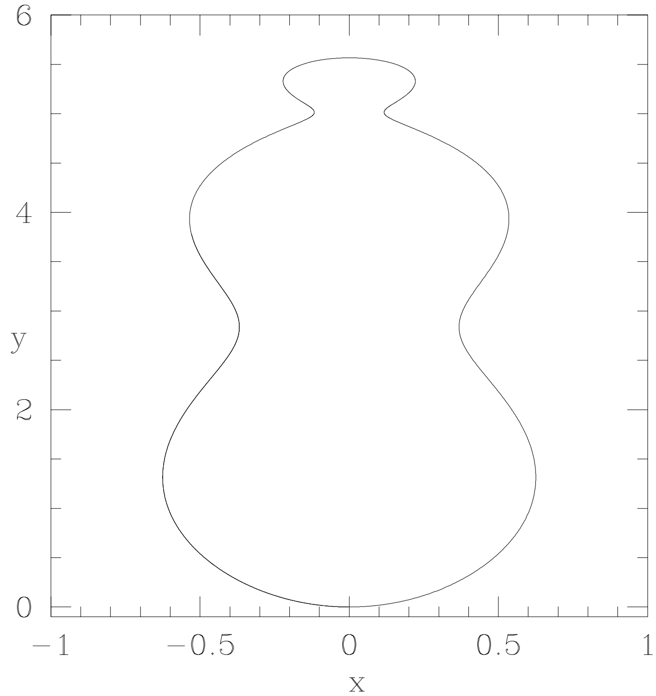

FIG. 10. Fixed point orbit, $k^2\Phi_0 = .5$, $\omega = 1/5$

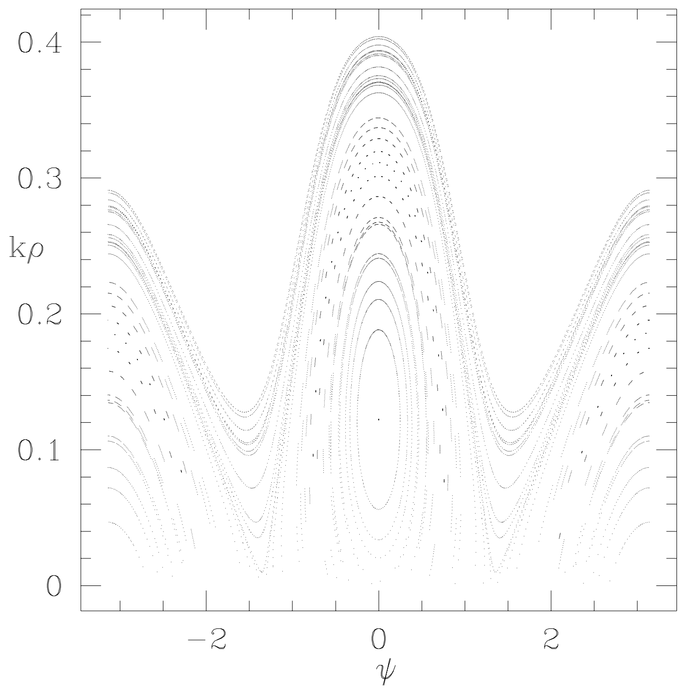

FIG. 11. Poincare, $k^2\Phi_0 = 0.2$, $\omega = 2/5$

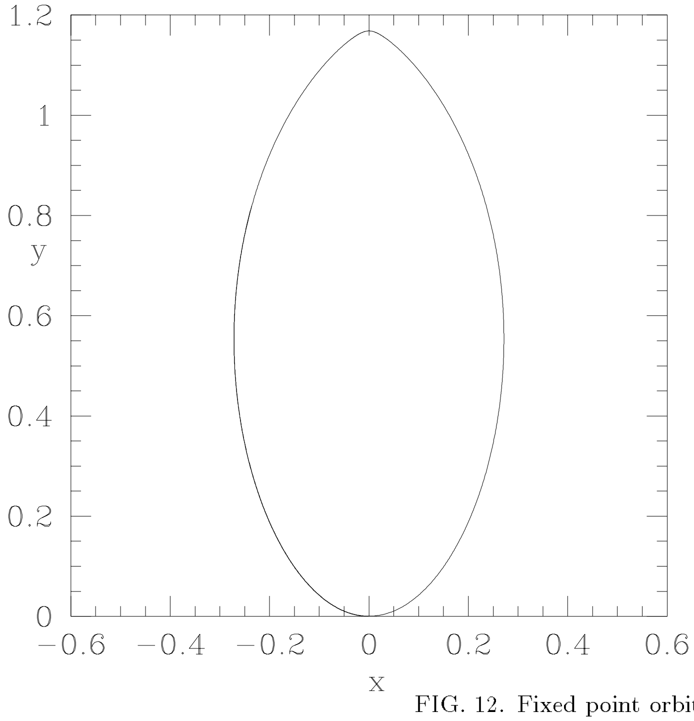

FIG. 12. Fixed point orbit, $k^2\Phi_0 = .2$, $\omega = 2/5$

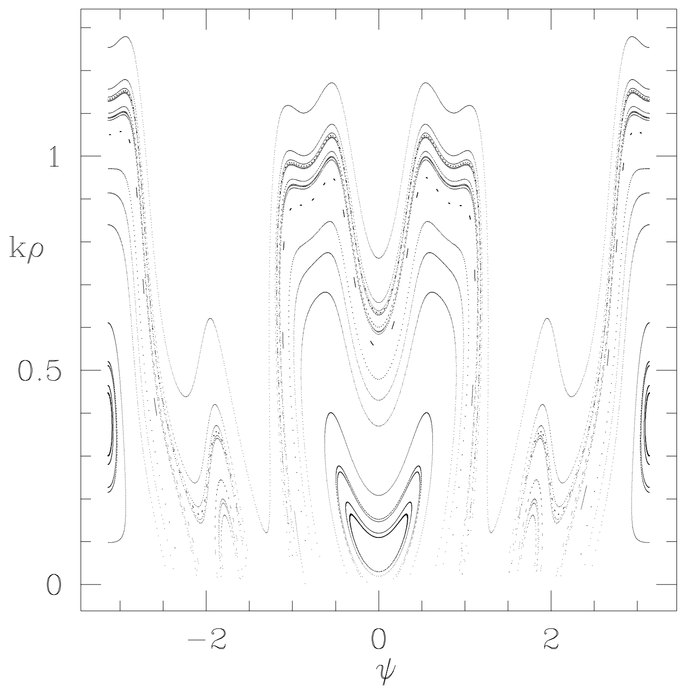

FIG. 13. Poincare, $k^2\Phi_0 = 0.6$, $\omega = 2/5$

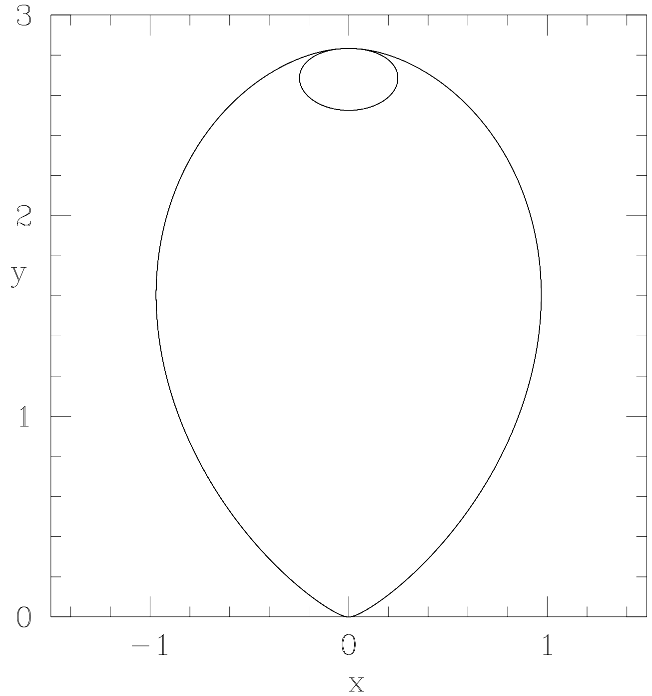

FIG. 14. Fixed point orbit, $k^2\Phi_0 = .6$, $\omega = 2/5$

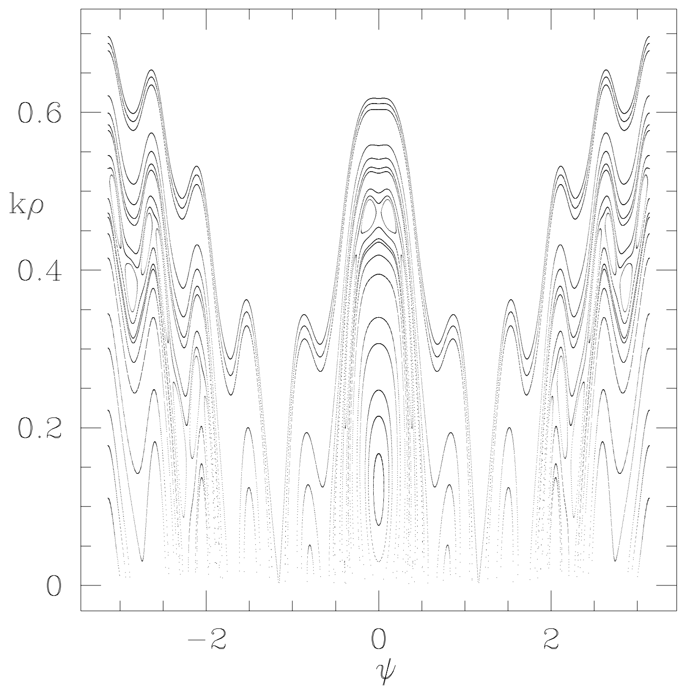

FIG. 15. Poincare, $k^2\Phi_0 = 0.6$, $\omega = 1/10$

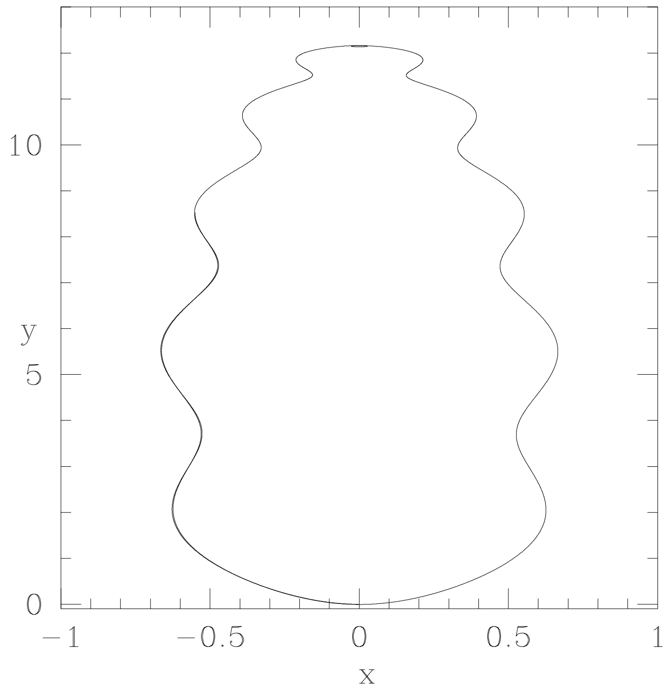

FIG. 16. Fixed point orbit, $k^2\Phi_0 = .6$, $\omega = 1/10$

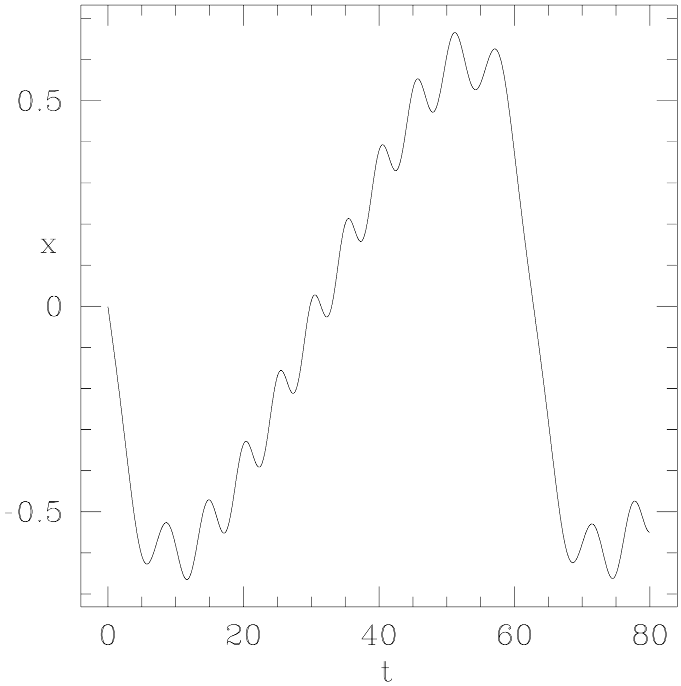

FIG. 17. Fixed point orbit, $k^2\Phi_0 = .6$, $\omega = 1/10$

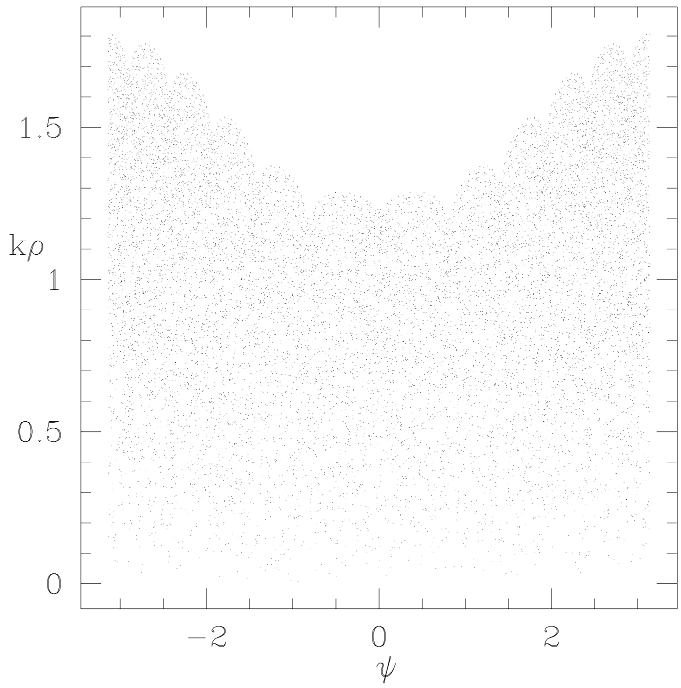

FIG. 18. Poincare, $k^2\Phi_0 = 1.$, $\omega = 1/10$

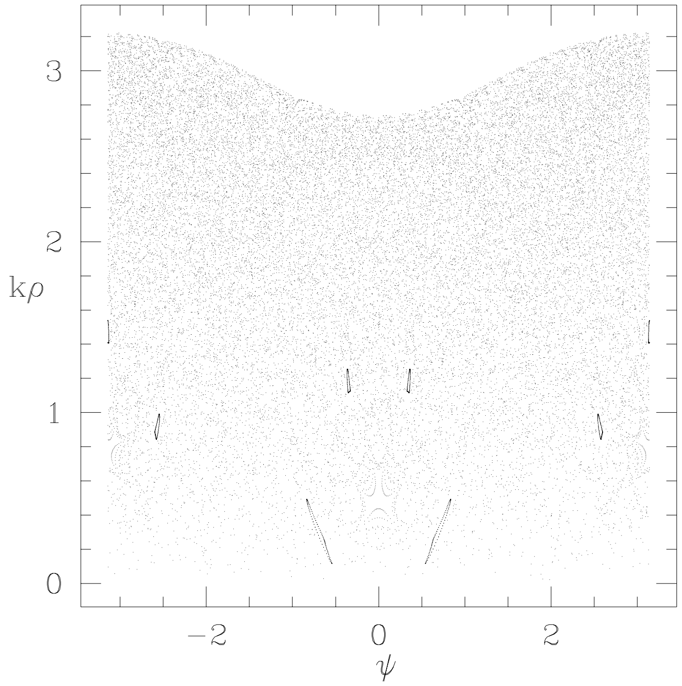

FIG. 19. Poincare, $k^2\Phi_0 = 1.$, $\omega = 1/2$

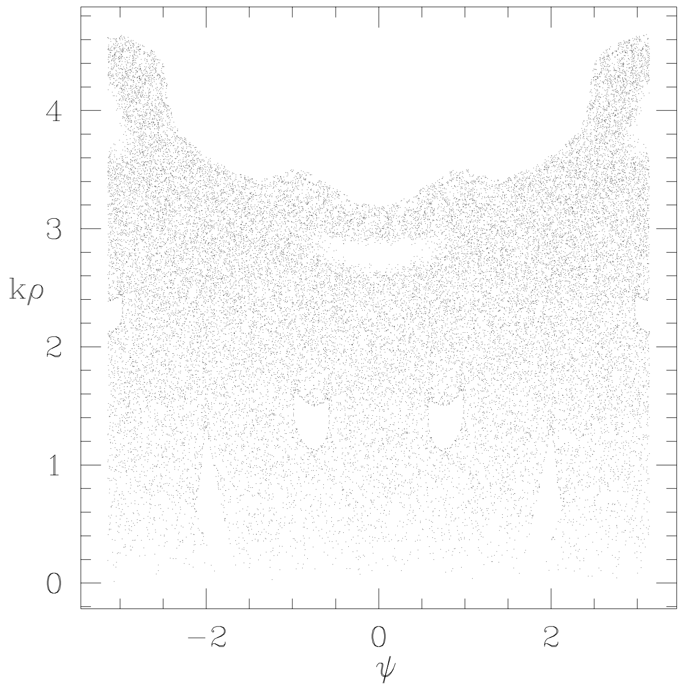

FIG. 20. Poincare, $k^2\Phi_0 = 2.$, $\omega = 1/2$

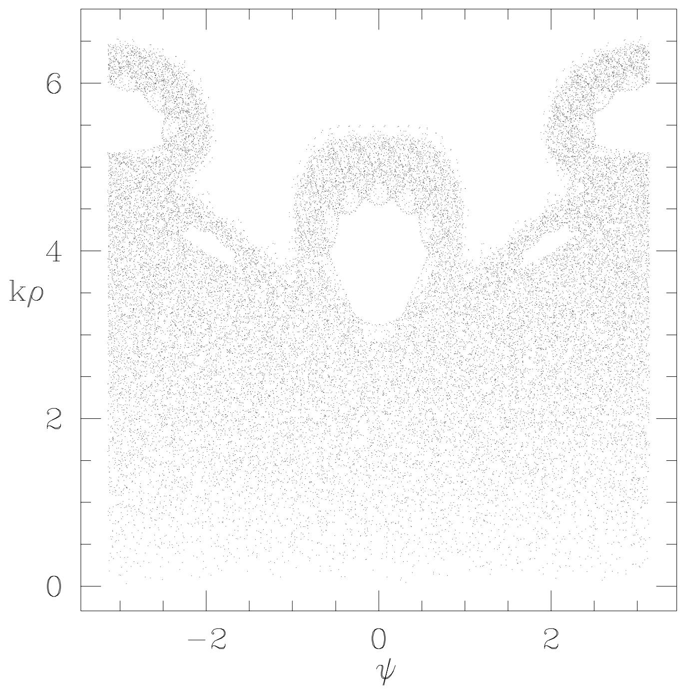

FIG. 21. Poincare, $k^2\Phi_0 = 3.$, $\omega = 1/2$

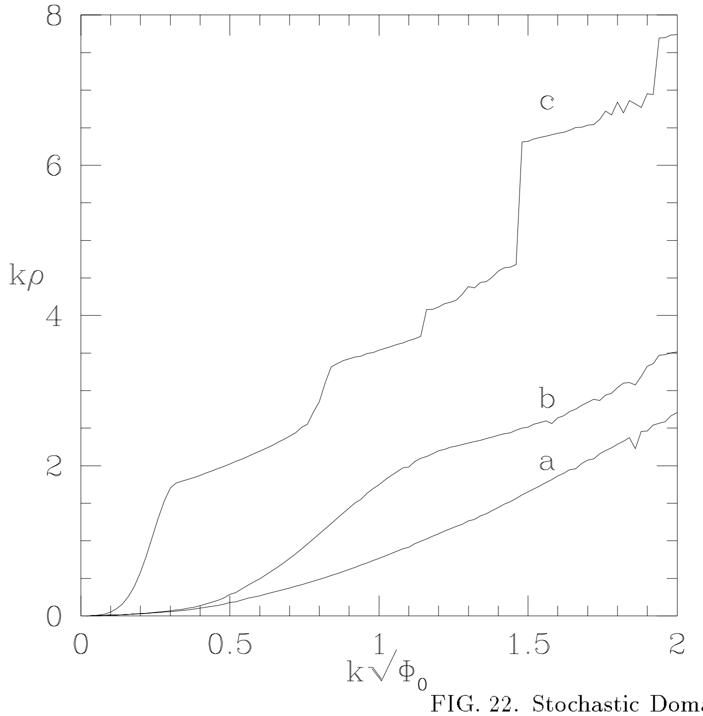

FIG. 22. Stochastic Domain vs $k\sqrt{\Phi_0}$, $\omega = 1/2$

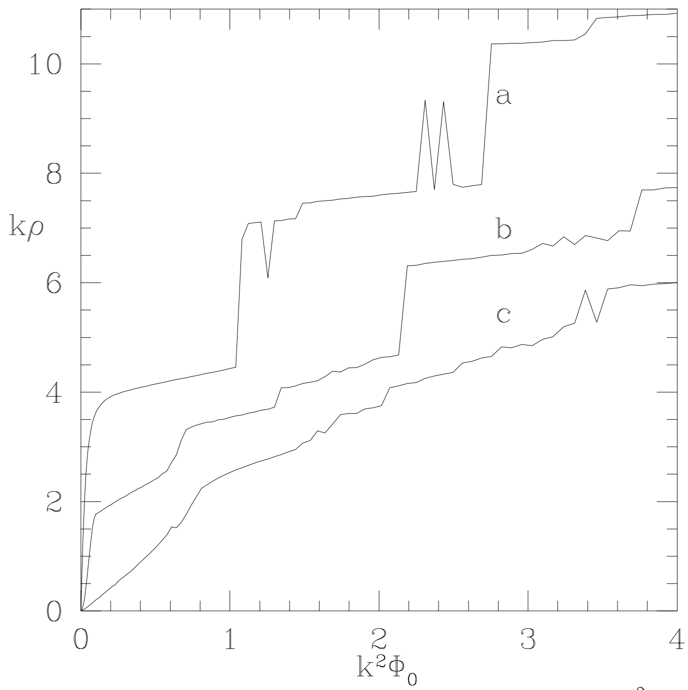

FIG. 23. Heating Domain vs $k^2\Phi_0$, a) $\omega = 1$, b) $\omega = 1/2$, c) $\omega = 1/5$.

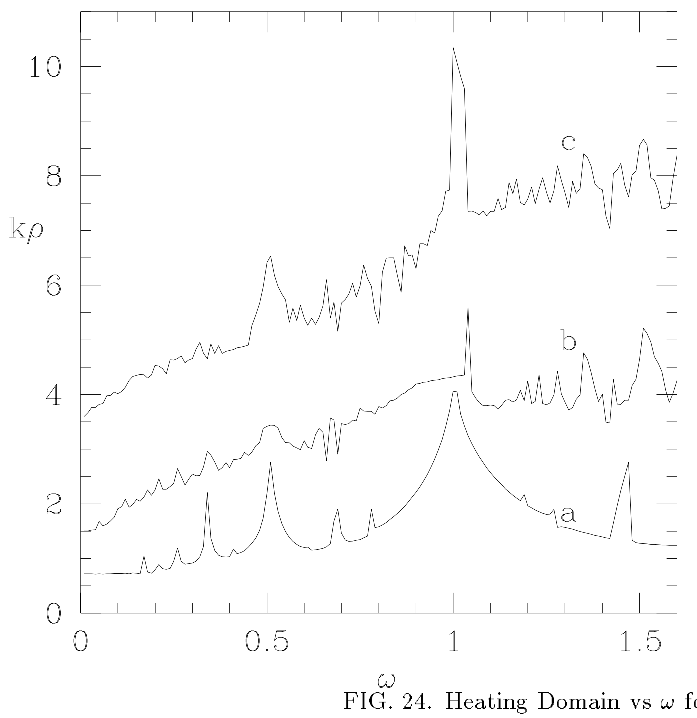

FIG. 24. Heating Domain vs ω for $k^2\Phi_0 =$ a)0.36, b) 0.8 c) 2.6

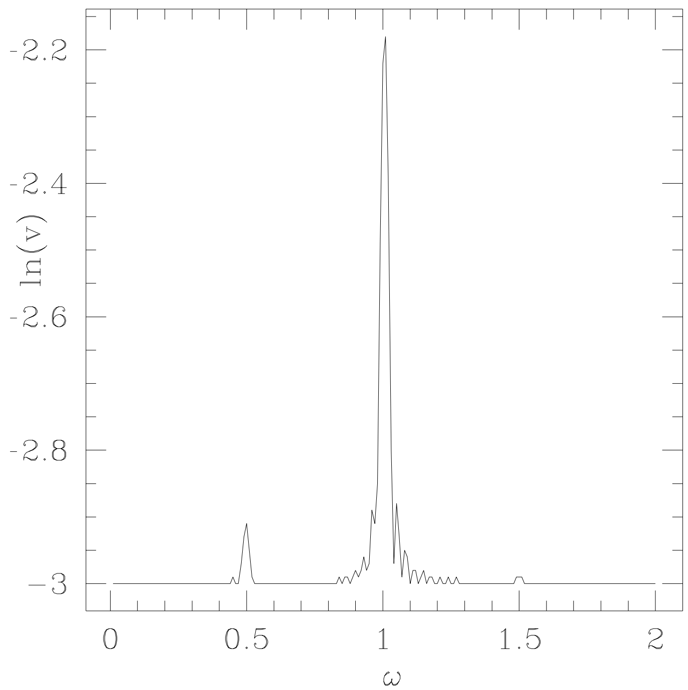

FIG. 25. Spectrum of velocity, $k^2\Phi_0 = 0.1$, $\omega = 1/2$

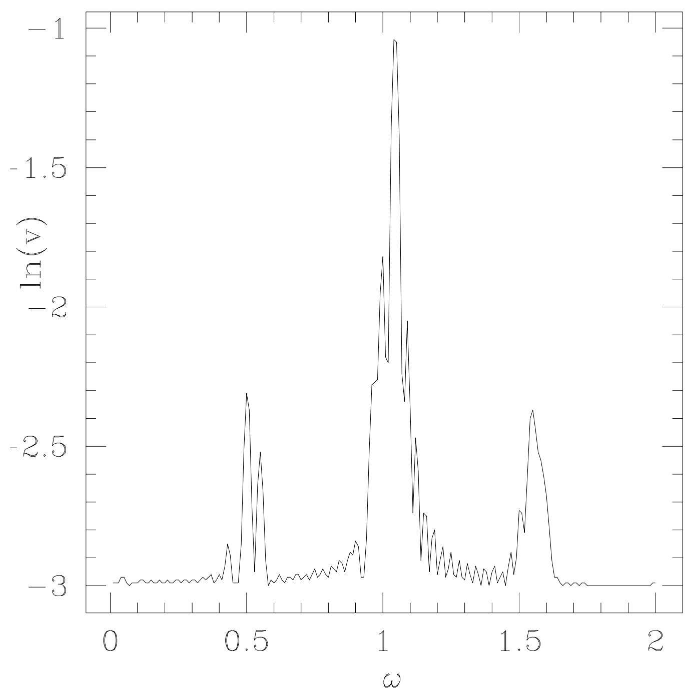

FIG. 26. Spectrum of velocity, $k^2\Phi_0 = 0.5$, $\omega = 1/2$

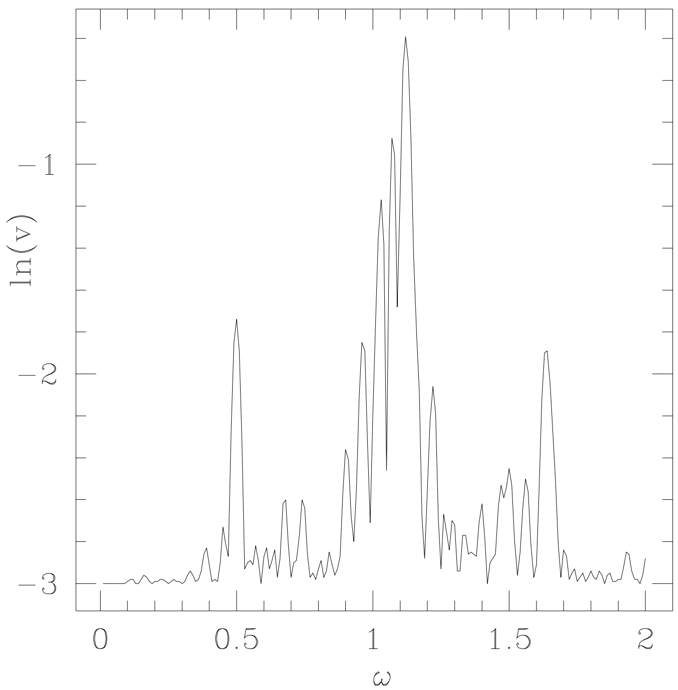

FIG. 27. Spectrum of velocity, $k^2\Phi_0 = 1.$, $\omega = 1/2$

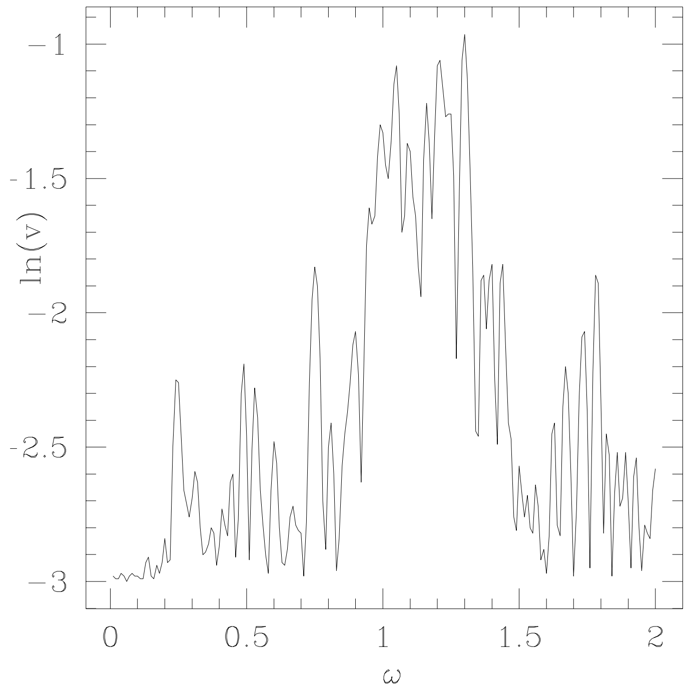

FIG. 28. Spectrum of velocity, $k^2\Phi_0 = 2.$, $\omega = 1/2$

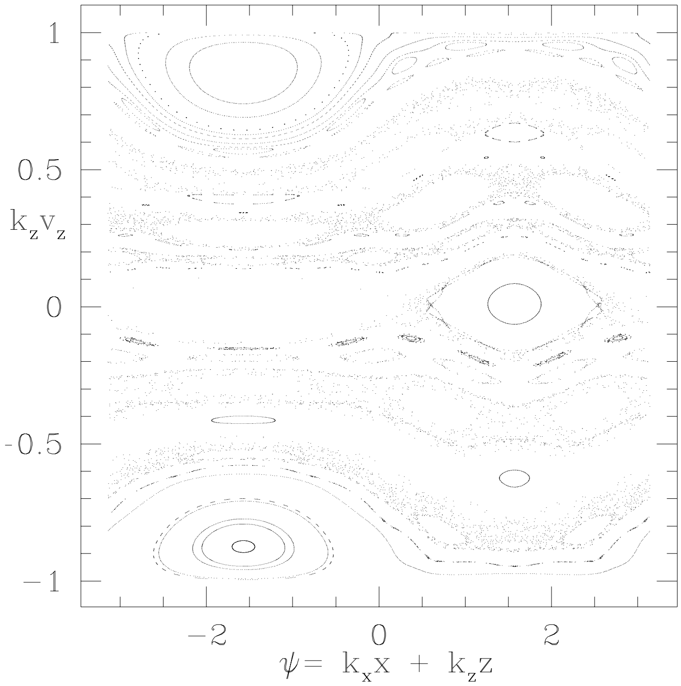

FIG. 29. Poincaré, $k_x v = 0.1$, $B_w = 0.22$.

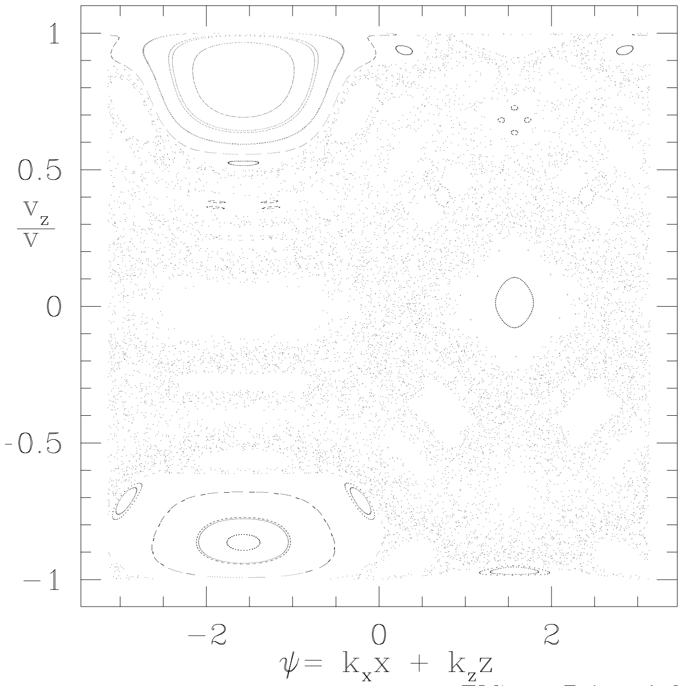

FIG. 30. Poincaré, $k_x v = 0.1$, $B_w = 0.3$.

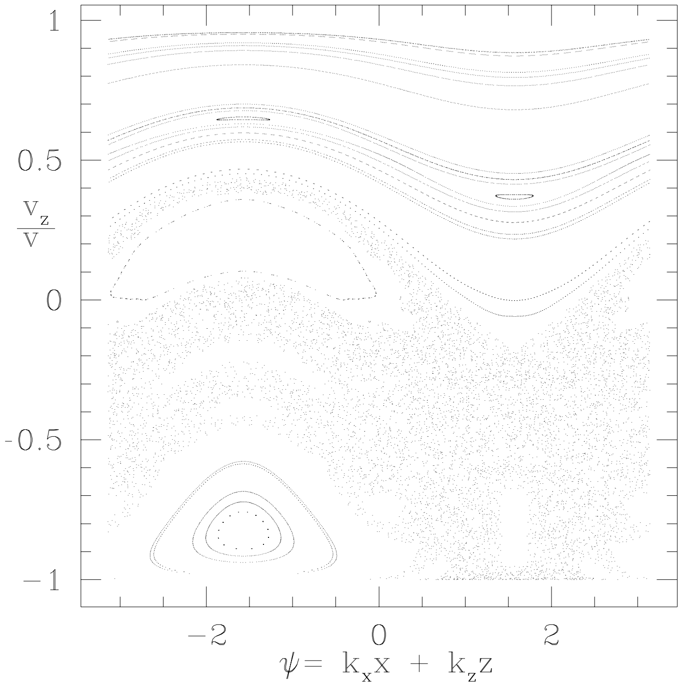

FIG. 31. Poincaré, $k_x v = 0.1$, $k_z v = 0.5$ $B_w = .3$.

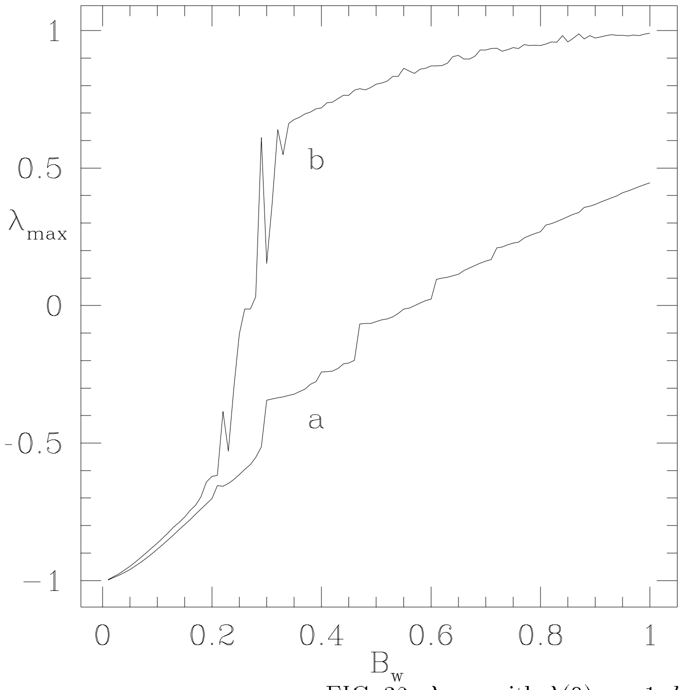

FIG. 32. λ_{max} with $\lambda(0) = -1$, $k_z v = 0.5$, and $k_x v = a)0.1, b)0.2$.

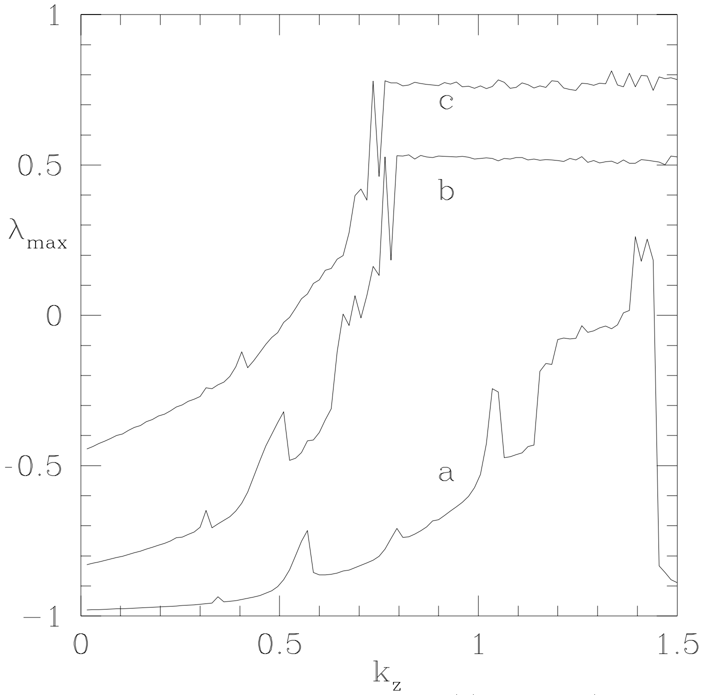

FIG. 33. λ_{max} with $\lambda(0) = -1$, $k_x/k_z = .2$, and a) $B_w = 0.1$, b) $B_w = 0.3$, c) $B_w = 0.6$